Moroccan Journal of Chemistry
ISSN: 2351-812X
http://revues.imist.ma/?journal=morjchem&page=login
Khaldan & al. / Mor. J. Chem. 8 N°1 (2020) 527-539

Combined 3D-QSAR Modeling and Molecular Docking Study on metronidazole-triazole-styryl hybrids as antiamoebic activity

Ayoub Khaldan[a], Khalil El khatabi[a], Reda El-mernissi[a], Abdelouahid Sbai[a,]*, Mohammed Bouachrine[a,b] and Tahar Lakhlifi[a]

[a]*Molecular Chemistry and Natural Substances Laboratory, Faculty of Science, Moulay Ismail University of Meknes, Morocco*

[b]*EST Khenifra, Sultan Moulay Sliman University, Benimellal, Morocco*

** Corresponding author:* a.sbai@umi.ac.ma;

Received 07 Jan 2020,
Revised 26 April 2020,
Accepted 26 April 2020.

Abstract

A series of twenty-two metronidazole-triazole-styryl hybrids as antiamoebic agents were studied based on the combination of 3D-QSAR and molecual docking. The CoMFA and CoMSIA models were carried out using eighteen compounds in the training set and four compounds in the test set gives Q^2 values of 0.684 and 0.664 respectively, and R^2 values of 0.882 and 0.894 respectively. The adapted alignment method with the suitable parameters resulted in reliable models. Based on contour maps produced by the CoMFA and CoMSIA models, we suggested new compounds with high predicted activities, Surflex-docking revealed the important interactions between the ligand and receptor. Therefore, it confirmed the stability of predicted molecules in the receptor with PDB code: 4CCQ.

Keywords: *3D-QSAR, CoMFA, CoMSIA, Molecular docking, Antiamoebic, Entamoeba histolytica, metronidazole, triazole.*

1. Introduction

Protozoan parasites have been causing serious problems to human health and are responsible for the high mortality and morbidity affecting more than 500 million people in the world [1]. Among protozoal infections, amoebiasisis the third leading cause of death. It is caused by the protozoa *Entamoeba histolytica* which is affects 50 million individuals per year [2]. The parasite affects the gastrointestinal tract of humans and reasons invasive infections and induces tissue destruction, creating amoebic colitis, dysentery and liver abscesses [3]. The 5-nitroimidazole class of compounds has long time employed for the treatment of protozoal infections. Amid the nitro-imidazole class of compounds, metronidazole (MTZ) is regarded the medicament of choice for the treatment of amoebiasis [4].The nitro group in the metronidazole nucleus is essential for its anti-amoebic activity. Reduction of the nitro group to the nitro radical anion by electron carriers in an anaerobic environment leads to breakdown to form toxic metabolites, which reason DNA damage and nonspecific macromolecular damage leading to cell death [5]. Nonetheless, this medicament is associated with certain grave side effects such as seizures, ataxia, genotoxicity, gastric mucus irritation, spermatozoid damage and hematuria, carcinogenicity [6-7]. Furthermore, there are reports of defeat of treatment with metronidazole due to the development of resistance by the parasite towards MTZ [8-9]. So there is a necessity to develop novel anti-amoebic agents with increased efficiency and with no side effects. The two sites in the metronidazole moiety viz. the ethyl hydroxy side chain and the methyl group attached to the imidazole ring can be chemically modified to get a diversity of compounds for the biological activity evaluation. In this paper, we advanced a quantitative structure-activity relationship (QSAR) model to suggest new effective potent drugs. QSAR methodology is a crucial implement in modern medicinal chemistry. It attempts to associate the biological activity of a series of chemicals to their physicochemical and structural properties relying on the hypothesis that similar structures have similar properties and that the more differences there are between molecules, the difficult it is to correlate their physicochemical properties and biological activities, whilst such correlations between highly similar molecules are much easier [10]. The application of QSAR to molecular modeling and drug design has directed to the addition of implements developed in the domain of computational chemistry. They have been employed to predict a wide number of biological endpoints and highlight on the reaction mechanism, if it is toxicological or pharmacological [11]. In this regard, comparative molecular field analysis (CoMFA) [12] and comparative molecular similarity indices analysis (CoMSIA) [13] were carried out to predict the activity of twenty-two metronidazole-triazole-styryl hybrids compounds got from literature, present antiamoebic activity [14], therefore suggest new qualified drugs against Entamoeba histolytica. Further, the surflex-docking method was performed to study the interactions of compound **17** (inactive molecule) and compound **8** (active molecule) with the suggested compounds to affirm the stability of 3D QSAR models developed. According on the CoMFA and CoMSIA models and docking results, a new active molecule was designed.

2. Materials and methods

A database of twenty-two compounds obtained from literature [15] consisted of novel metronidazole-triazole-styryl hybrids, the data set was split into two sets, eighteen compounds were selected as training set and four compounds were selected as test set, relying on a random selection to assess the capability of the got model. The biological activities of both the training and test set molecules and their structures are exposed in table 1. This data is employed to build 3D-QSAR model and to examine their physicochemical properties. For the QSAR analysis the in vitro biological activities IC_{50} (µM) were transformed into the corresponding pIC_{50} values (i.e. pIC_{50} is the negative logarithm of IC_{50}, ($pIC_{50} = -\log_{10}(IC_{50})$). 3D structure constructing and all modeling were employed employing the Sybyl 2.0 program package.

Table 1. Chemical structures and antiamoebic activities of metronidazole-triazole-styryl hybrids

Compound	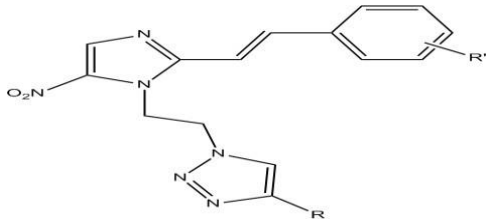		IC_{50} (µm)	pIC_{50}
	R	R’		
1*	CH_2OH	H	1,12	5,950
2	CH_2OH	4-F	0,18	6,744
3	CH_2OH	4-Cl	1,11	5,954
4	CH_2OH	4-Br	1,65	5,782
5*	CH_2OH	4-CH_3	2,13	5,671
6*	CH_2OH	4-CH_2CH_3	4,18	5,378
7	C_6H_5	H	1,35	5,869
8	C_6H_5	4-F	0,12	6,920
9	C_6H_5	4-Cl	1,22	5,913
10	C_6H_5	4-Br	1,77	5,752
11	C_6H_5	4-CH_3	2,51	5,600
12	C_6H_5	4-CH_2CH_3	4,68	5,329
13	2-pyridyl	H	5,13	5,289
14	2-pyridyl	4-F	0,13	6,886
15	2-pyridyl	4-Cl	0,29	6,537
16	2-pyridyl	4-Br	1,1	5,958
17	2-pyridyl	4-CH_3	6,01	5,221
18	$CH_2OC_6H_5$	H	3,56	5,448
19	$CH_2OC_6H_5$	4-F	0,28	6,552
20*	$CH_2OC_6H_5$	4-Cl	0,35	6,455
21	$CH_2OC_6H_5$	4-Br	1,68	5,774
22	$CH_2OC_6H_5$	4-CH_3	5,38	5,269

* Test set molecules

2.1. Minimization and alignment

Molecular structures were sketched with sketch module in SYBYL program and optimized using the standard Tripos molecular mechanics force field [16] with Gasteiger-Hückel charges [17] by conjugated gradient technique with gradient convergence criterion(0.01 kcal/mol). Simulated annealing on the optimized structures was performed with 20 cycles. The molecular alignment is the second step used to develop a performing 3D-QSAR model. Figure 1 shows the 3D structure of the core and superimposed structures of aligned data set, the data set was aligned by distill alignment technique available in SYBYL [18] utilizing the more active compound (molecule **8**) as template.

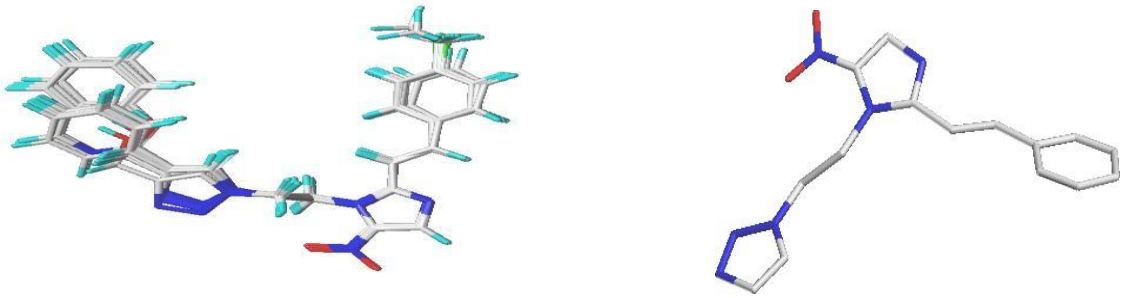

Aligned compounds Core

Figure1. 3D-QSAR structure superposition and alignment of training set employing compound **8** as a template.

2.2. 3D QSAR Studies

To define the contributions of steric, electrostatic, hydrophobic, acceptor and donor fields of the data set and to construct predictive 3D- QSAR models, CoMFA and CoMSIA studies were employed relying on the molecular alignment methods. These studies were performed as earlier reported in the literature [19].

2.3. CoMFA and CoMSIA

The CoMFA [12] model was carried out to assess steric and electrostatic energies of the Tripos force fields implemented in SYBYL-X 2.0, also attempts to establish relationships between these quantities and the measured activity. The aligned database was applied in a three dimensional regularly with a grid spacing of 2 Å in all Cartesians directions. A carbon atom with an atomic radius of 1.52 Å and charge +1 was used as a probe to calculate the potentials, which was positioned at each lattice point of the grid box to generate, respectively, the electrostatic and steric fields, these last two, energy cut-off value was set by default at 30 kcal/mol [20]. In the case of the CoMSIA [13] model was performed in SYBYL-X 2.0, utilizing the same grid box as employed in CoMFA computation, and the same training and test sets. Five fields' namely electrostatic, steric, hydrophobic effect and hydrogen bond acceptor and donor were calculated from analogous actives molecules, to improve a CoMSIA model. For the computation of hydrophobic and hydrogen-bond potentials, a probe atom with hydrophobicity +1 and hydrogen bond donor/hydrogen bond acceptor of +1 was employed, the attenuation factor was set by default at 0.3 [21].

2.4. Partial least square (PLS) analysis

PLS method [22] employed in deriving the 3D-QSAR models is an expansion of multiple regression analysis in which the original variables are superseded by a small set of their linear combinations. In this rapport, PLS technique with leave-one-out (LOO) cross-validation is applied to determine the optimal numbers of components based on cross validation coefficient Q^2. Further, an external validation is carried out employing a test set of four molecules. The final analysis is performed to obtain correlation coefficient R^2 and Q^2 values, whereas Q^2 determines the internal predictive capability of the model, and R2 value assesses the internal consistency of the model. Consequently, the better QSAR model is selected based on a combination of R^2 and Q^2.

2.5. Y-Randomization Test

Y-Randomization was applied to affirm the got models [23]. The Y vector ($-\log IC_{50}$) is arbitrarily shuffled several times and after every test, a new QSAR model is constructed. The new QSAR models are predictable to have feeble values of R^2 and Q^2 than those in the original models. Then, this technique was carried out to avoid the possibility of

the chance correlation. If high values of the Q^2 and R^2 are getting, it means that an acceptable 3D-QSAR model can't be produced for this data set because of the structural redundancy and chance correlation

2.6. Molecular Docking

To recognize of the feeble-energy binding modes of a small molecule (or ligand) in the active site of a macromolecule (or receptor), molecular docking method was performed. In sum, the molecular docking process commence by the algorithms posing the small ligand in a selected binding site of the target macromolecule, which can donate different conformations of the ligand. Further, the interactions between the ligand and the macromolecule are assessed with scoring functions to estimate the binding energy and finally recognize the optimal binding mode [24]. In present study, this technique was carried out using Surflex-dock available in SYBYL-X.2.0.This latter was performed for the preparation steps of proteins and ligands for the docking protocol. Furthermore, Discovery Studio 2016 [25] and PyMol [26] software's were applied to analyze the get results.

2.6.1. Macromolecule preparation

The 3D crystal structure of *E. histolytica* thioredoxin reductase (EhTrR) protein was downloaded from the Protein Data Bank (http://www.rcsb.org), (PDB entry code: **4CCQ**) [27]. No one of the understudy ligands is complexed with this protein in PDB, so, its original ligand was detached. The PDB file was prepared by Discovery Studio 2016, such as all ligands, co-factors and solvent molecules were detached from the model. Previously docking, hydrogen atoms of the receptor were additional to the prepared structure. The definition of active site definition was carried out founded on the original ligand in the crystal. We chose molecule **8** as the subject to dock into the active pocket under the conditions previously mentioned [28].

2.6.2. Ligand preparation

For docking study, the 3D structures of ligands (compounds **8**, **17** and proposed compound **X1**) were construct using the SKETCH option in SYBYL, Moreover, they were minimized under the Tripos standard force field [16] with Gasteiger-Hückel charges [17] by conjugated gradient method with gradient convergence criterion of 0.01kcal/mol Å in SYBYL software.

3. Results and discussion

3.1. CoMFA results

PLS summary shows that CoMFA model has high R^2 (0.882) and four optimum number of components, small estimation error Scv (0.222), F (24.386) values, the cross-validated determination coefficient Q^2 (0.684). The external predictive ability of QSAR model is usually cross checked and validated using test sets. The four randomly selected test sets-were optimized and aligned in the same manner as training sets. The external validation gave high value of $Rtest^2$ (0.978) demonstrating that prediction capability of CoMFA model is tolerable. Moreover the rations of steric and electrostatic contributions were almost found to be 50:50 which show that steric and electrostatic interactions are same important.

3.2. CoMSIA results

Founded on CoMSIA descriptors available on SYBYL a 3D-QSAR model was suggested to elucidate and predict quantitatively the Steric, Hydrophobic, Electrostatic, donor and acceptor field's effects of substituents on the anti-amoebic activity of a series of metronidazole-triazole-styryl hybrids. The obtained statistical keys for the CoMSIA

model, as R^2, Q^2, R $test^2$, F-test, and Scv were determined by SYBYL are display in table 2. Several combinations of the five fields were produced. Table 2 show that CoMSIA developed model has high Cross and non-cross validated correlation coefficients with Q^2 (0.664) and R^2 (0.894) respectively, The F-test value (27.418) values, Standard error estimation S_{cv} obtained has a low value 0.211 and the optimal number of principal components employing to produce the CoMSIA model is 4, which is reasonable considering the number of molecules employed to construct the model. Finally, the prediction capability of the suggested model is affirmed by using the external validation, the $Rtest^2$ value obtained is 0.976. These statistics results demonstrated the good stability and the powerful predictive capability of CoMSIA model.

Table 2. PLS Statistics of CoMFA and CoMSIA models.

							Fractions				
Model	Q^2	R^2	Scv	F	N	$Rtest^2$	Ster	Elec	Acc	Don	Hyd
CoMFA	0.684	0.882	0.222	24.386	4	0.978	0.506	0.494	-	-	-
CoMSIA	0.664	0.894	0.211	27.418	4	0.976	0.077	0.519	0.044	0.154	0.206

Q^2: Cross-validated determination coefficient, N: Optimum number of components, R^2: Non-cross- validated determination coefficient, Scv: Standard error of the estimate.;F: F-test value;$Rtest^2$: External validation determination coefficient

Table 3. Antiamoebic and the predicted activities of metronidazole-triazole-styryl hybrids.

N°	pIC_{50}	CoMFA		CoMSIA	
		Predicted	Residuals	Predicted	Residuals
1*	5,950	5.899	0.051	5.877	0.073
2	6,744	6.638	0.106	6.641	0.103
3	5,954	5.834	0.120	5.832	0.122
4	5,782	5.640	0.142	5.635	0.147
5*	5,671	5.581	0.090	5.592	0.079
6*	5,378	5.502	-0.124	5.505	-0.127
7	5,869	5.598	0.271	5.594	0.275
8	6,920	6.786	0.134	6.785	0.135
9	5,913	6.049	-0.136	6.056	-0.143
10	5,752	5.852	-0.100	5.860	-0.108
11	5,600	5.095	0.505	5.099	0.501
12	5,329	5.160	0.169	5.179	0.150
13	5,289	5.528	-0.239	5.518	-0.229
14	6,886	6.806	0.080	6.807	0.079
15	6,537	6.152	0.385	6.152	0.385
16	5,958	5.993	-0.035	5.995	-0.037
17	5,221	5.247	-0.026	5.247	-0.026
18	5,448	5.381	0.067	5.390	0.058
19	6,552	6.525	0.027	6.525	0.027
20*	6,455	6.491	-0.036	6.496	-0.041
21	5,774	5.646	0.128	5.646	0.128
22	5,269	5.066	0.203	5.062	0.207

* Test set molecule

The correlations of predicted and observed pIC_{50} values are illustrated in figure 2.

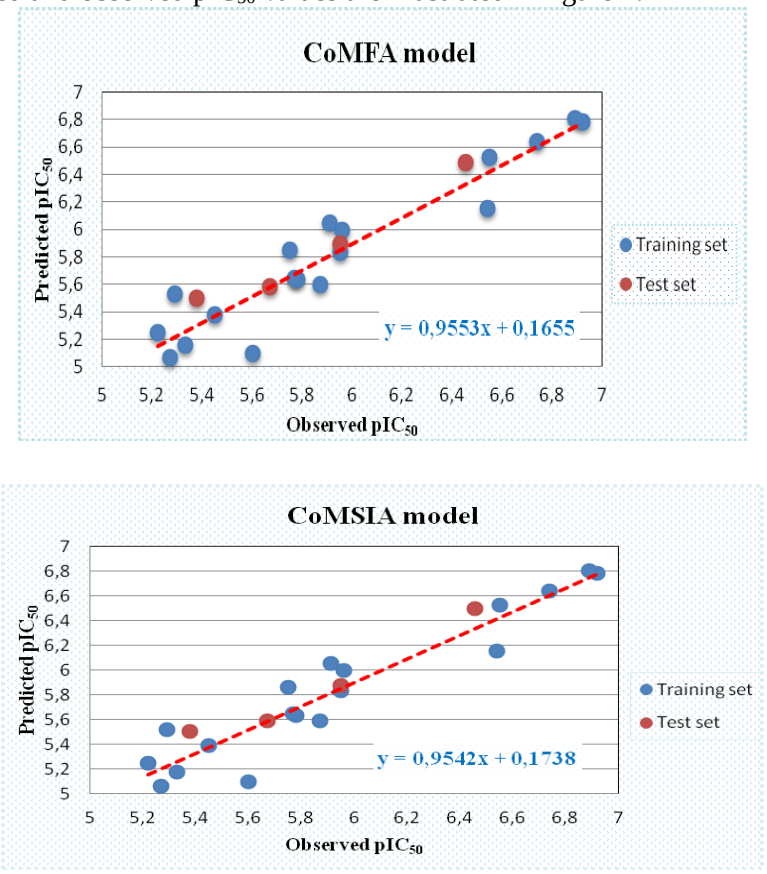

Figure 2. Experimental versus predicted activity of the training and test set relying on the CoMFA and CoMSIA model.

According to the figure 2 we notice a regular distribution of activity values depending on the experimental values. Moreover, CoMFA and CoMSIA almost have the same determination coefficient R^2, cross-validated determination coefficient Q^2 and $Rtest^2$. Concerned the value of the standard error, we notice that CoMFA model has a high Scv CoMSIA's model that is showed in figure 2.

3.3. Graphical Interpretation of CoMFA and CoMSIA results

CoMFA and CoMSIA contour maps were produced to streamline regions where the activity can be decreased or increased. CoMFA contours are illustrated in figure 3 (a, b), whereas CoMSIA contours are displayed in figure 4 (a, b, c, d, e), in this study, compound **8** was employed as a reference structure.

3.4. CoMFA Contour Maps

CoMFA steric interactions are presented with green and yellow colors (figure 3a), while electrostatic interactions are displayed with red and blue colored contours (figure 3b). The bulky substituents are favored around green regions, whereas yellow regions bulky substituents are unflavored. Further, the blue regions show that nucleophilic groups are preferred, while, and in the red regions are unflavored.

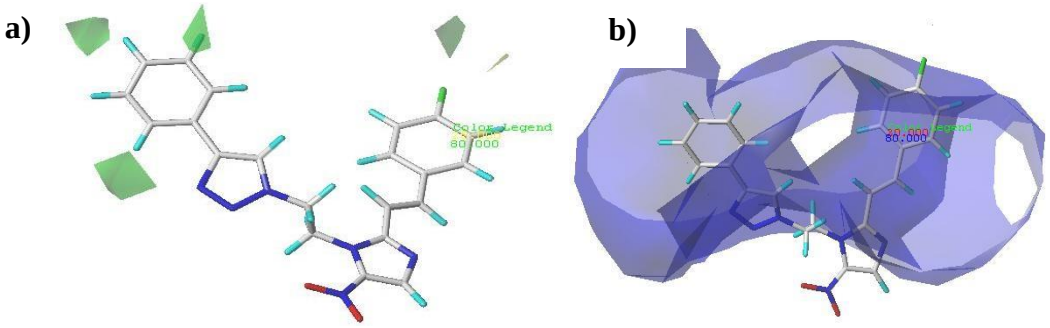

Figure 3. Std* coeff. Contour maps of CoMFA analysis with 2 Å grids spacing in combination with compound **8**. **a**) Steric fields: yellow contours (20% contribution) show regions where voluminous groups are required to decrease the activity, while green contours (80% contribution) demonstration regions where huge groups are required to increase the activity. **b**) Electrostatic fields: blue contours (80% contribution) show regions where groups with positive charges improve the activity, whereas red contours (20% contribution) demonstration regions where groups with negative charges improve the activity.

The figure 3a show, the green regions near to fluorine atom and around *ortho*, *meta* and near to *para* positions of phenyl groups indicate that bulky groups in these positions can improve the activity of the molecules. Whereas figure 3b indicates that addition of groups with negative charges in R position can increase the potency.

3.5. CoMSIA Contour Map

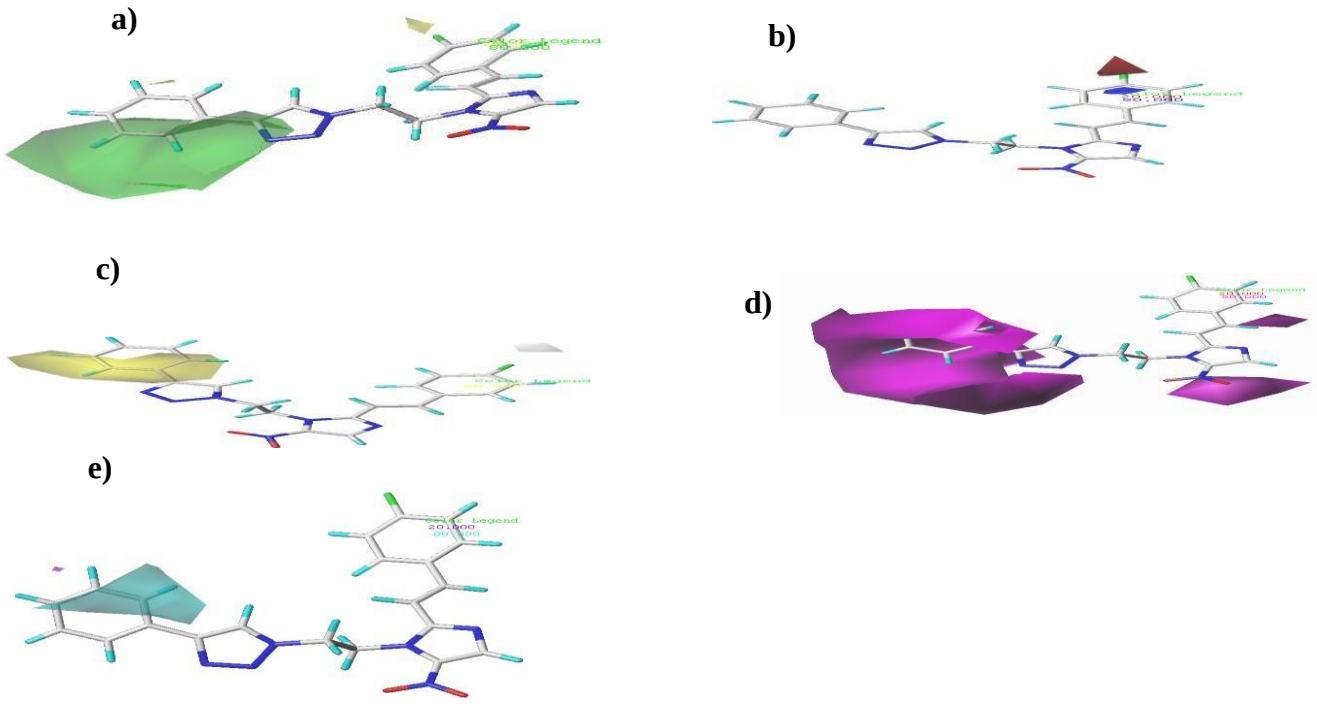

Figure 4. Contour maps of CoMSIA analysis with 2 Å grids spacing in combination with compound **8.a)** steric fields: yellow contours (20% contribution) designate regions where huge groups decrease activity, whereas green contours (80% contribution) designate regions where huge groups improve the activity, **b)** Electrostatic fields: red contours (20% contribution) demonstration regions where electron-withdrawing groups growth activity; blue contours (80%

contribution) demonstration regions where electron- withdrawing groups reduce activity, **c)** Hydrophobic fields: white contours (20% contribution) designate hydrophobic groups are unfavorable, whereas yellow contours (80% contribution) demonstration hydrophobic groups are preferred, **d)** H-bond acceptor fields: Magenta contours (80% contribution) show regions where an H-bond acceptor substituents improve the activity; red contours (20% contribution) designate regions where H-bond acceptor substituents reduce the activity. **e)** H- bond donor fields: Cyan contours (80% contribution) show regions where H-bond donor group's growth activity while purple contours (20% contribution) show regions where H-bond donor substituents reduce the potency.

The CoMSIA steric (Figure 4a) show, yellow contour near to the fluorine atom means that substitute bulky groups in this place may decrease the potency. Whereas the hug green contour around *ortho* and *meta* positions of phenyl groups and nitrogen of cycle triazolic explain that bulky groups in these positions would increase the activity. CoMSIA electrostatic (Figure 4b) indicate, red contour near to fluorine atom means that groups with electron-withdrawing character can increase the activity. CoMSIA hydrophobic (Figure 4c) designate, yellow contour around *ortho*, *meta* and *para* positions of phenyl groups indicate that replacing these positions with hydrophobic groups may increase the activity. While white contour near to fluorine atom indicates that hydrophobic groups are unflavored. CoMSIA H-bond acceptor (Figure 4d) indicates, magenta contour around *meta* and *para* positions of phenyl group, nitrogen dioxide and hydrogen of styryl group revealed a hydrogen bond acceptor substituent at these positions can improve the potency. CoMSIA H-bond donor (Figure 4e) show, cyan contour around *ortho* position of phenyl group show a hydrogen bond donor substituent at this position are favorable.

3.6. Y-Randomization

Table 4. Q^2 and R^2 values after random Y-randomization tests

	CoMFA		CoMSIA	
Iteration	Q^2	R^2	Q^2	R^2
1	-0.178	0.729	-0.081	0.513
2	-0.115	0.447	-0.229	0.356
3	-0.424	0.419	-0.451	0.262
4	-0.305	0.616	0.002	0.556
5	-0.05	0.651	-0.195	0.521
6	-0.418	0.726	-0.507	0.779

To affirm the CoMSIA and CoMFA models, the Y-Randomization method is executed. Divers random shuffles of the dependent variable were carried out then after every shuffle, a 3D-QSAR was developed and the obtained results are illustrated in table 4. The weak Q^2 and R^2 values obtained after every shuffle showed that the good result in our original CoMFA and CoMSIA models are not due to a chance correlation of the training set.

3.7. New designed molecules

Based on the suggested 3D-QSAR (CoMFA/CoMSIA) models, three new metronidazole-triazole-styryl derivatives were designed (Table 5). The new predicted structure **X1** shows higher activity (pIC_{50} = 7.142 and pIC_{50} = 7.103 for CoMSIA and CoMFA models respectively) than compound **8** that's the more active molecule of the series (Figure 5). Additionally, these newly molecules were minimized and aligned to the database employing molecule **14**.

Table 5. Predicted pIC_{50} of newly designed compounds based on CoMFA and CoMSIA 3D-QSAR models.

	Predicted *pIC50*	
N°	**CoMFA**	**CoMSIA**
X1	7.103	7.142
X2	7.081	7.136
X3	7.110	7.104

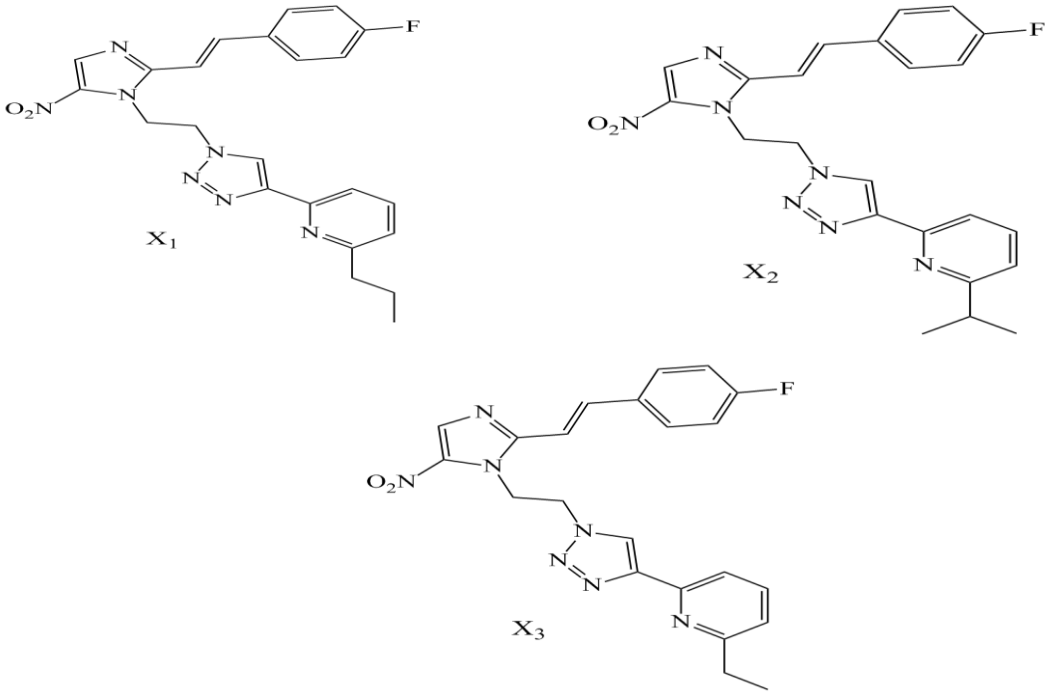

Figure 5. Structures of newly designed molecules.

3.8. Docking results

Surflex-dock was applied to explain the activity of the compounds, and its relation with the interactions between the active molecule (Compound **8**), the inactive molecule (Compound **17**) and the proposed molecule (Compound **X1**) with receptor (PDB ID: 4CCQ).

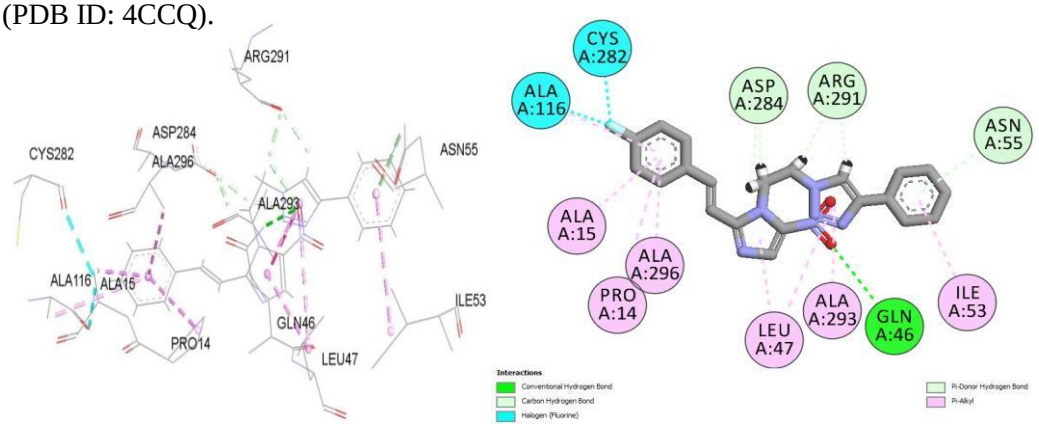

Figure 6a. Docking interactions between the protein 4CCQ and the compound **8** as the active compound in database.

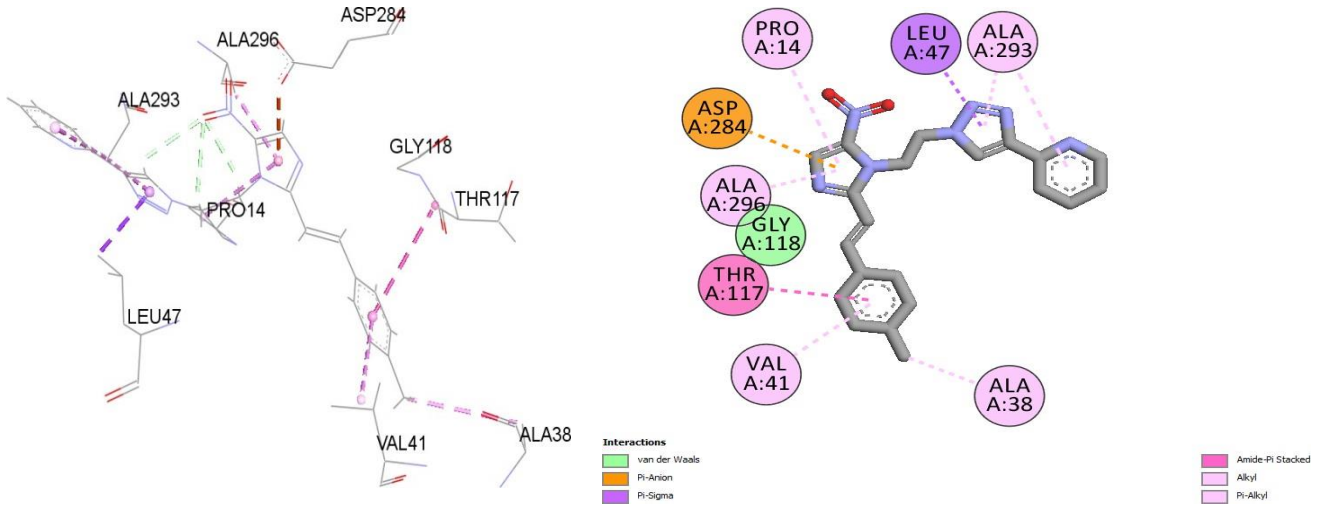

Figure 6b. Docking interactions between the protein 4CCQ and the compound **17** as the inactive compound in database.

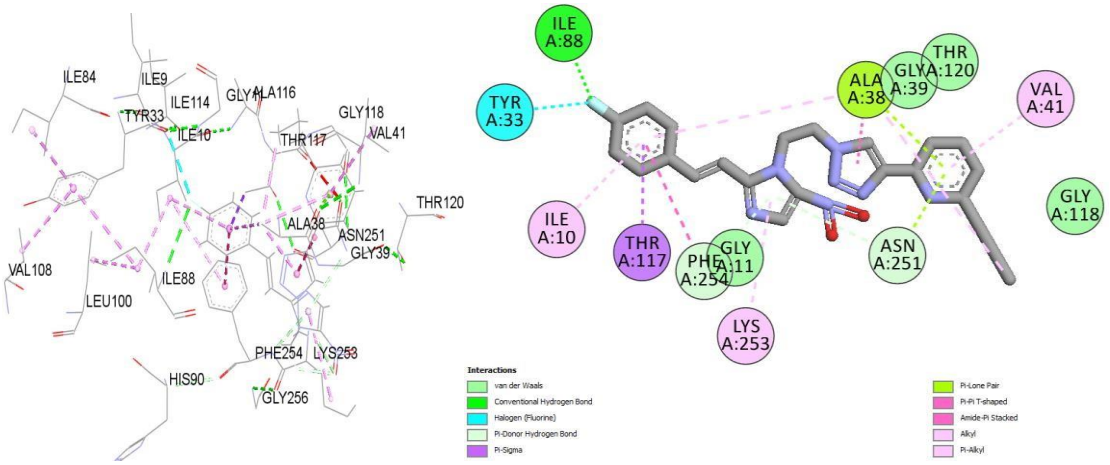

Figure 6c. Docking interactions between the protein 4CCQ and the proposed compound **X1**.

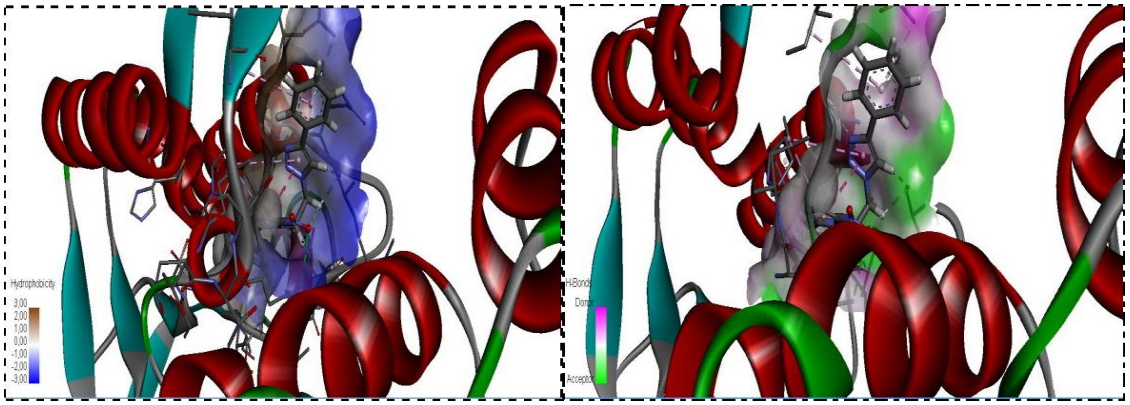

Figure 6d. The interaction H-bond and Hydrophobicity between the compound **8** (active molecule) and the protein 4CCQ, visualized with discovery studio visualizer program.

The figure 6a shows, the active molecule (Compound **8**) presents a pi-Donor hydrogen bond interaction with ASP A:284, ARG A:291 residues, carbon hydrogen bond interaction with ASN A:55 residue, halogen (Fluorine) interaction with ALA A:116, CYS A:282 residues, conventional hydrogen bond interaction with GLN A:46 residue, and pi-Alkyl interaction with ALA A:15, ALA A:296, PRO A:14, LEU A:47, ALA A:293, ILE A:53 residues. While the inactive molecule (Compound **17**), presents, pi-Sigma interaction with LEU A:47 residue, pi-Anion interaction with ASP A:284 residue, Amid-Pi stacked interaction with THR A: 117 residue, Alkyl interaction with PRO A:14, ALA A:296; ALA A:293, VAL A:41 residues, and Pi-Alkyl interaction with ALA A:38 residue (Figure 6b). Which means that group R in compound **8** (the active molecule) offers a lot of hydrogen bond than compound 17(the inactive molecule). Furthermore, the proposed compound **X1** affords Alkyl interactions with VAL A:41, ILE A:10 LYS A:253, ALA A:38 residues, pi-alkyl interaction with ALA A:38 residue, halogen (Fluorine) interaction with TYR A:33 residues, pi-donor hydrogen bond interaction with ASN A: 251, PHE A:254 residues, pi-Sigma interaction with THR A:117 residue, pi-pi-T-shaped interaction with PHE A:254 residue, amid-pi-stacked interaction with ALA A:38 residue. The fluorine atom offers a conventional hydrogen bond interaction with ILE A: 88 residue. ALA A:38 residue indicate the pi-lone pair interaction (Figure 6c). These interactions explain the stability and the high activity of the proposed compounds. Moreover, the figure 6d shows the green color around R group indicates the regions where H-bond acceptor are favored, while the brown color around R_1 group indicates the regions where hydrophobic groups are favored. In conclusion all these results have been used for the design of new molecules with high antiamoebic activity.

4. Conclusion

Different metronidazole-triazole-styryl analogues were identified as potentially effective oral antiamoebic agents through a series containing 22 molecules of computer-aided drug design procedures, such as molecular docking and 3D-QSAR modeling. CoMFA/CoMSIA models offered good internal and external validation capabilities with interesting statistical ability. Relying on their contour maps new powerful molecules were developed which showed high anti-amoebic activity. Further, molecular docking process was applied to study the possible binding modes with EhTrR receptor at the active pocket, and to identify the nature of interactions between ligands and residues. These results shown that the optimal CoMFA/CoMSIA models, molecular docking can be employed to predict novel anti-amoebic agents and guide the discovery of new potential analogues.

References

[1] E. C. Keen, Future Microbiol. 8 (2013) 821-823.

[2] J.D. Ospina-Villa, N.Guillén, C. Lopez-Camarillo, J. Soto-Sanchez, E. Ramirez-Moreno, R. Garcia-Vazquez, C.A. Castañon-Sanchez, A. Betanzos, L.A. Marchat, J. Microbiol. 55 (2017) 783-791.

[3] A.A. Kelsoa, S.D. Goodsona, S. Chavan, A.F. Saya, A. Turchicka, D. Sharma, L.L. Ledforda, E. Rattermana, K. Leskoskea, A.V. King, C.C. Attaway, Y. Bandera, S. H. Foulger, A.V. Mazin , L.A. Temesvari, M.G. Sehorna. Mol. Biochem. Parasitol. 210 (2016) 71–84.

[4] S.M. Townson, P.F.L. Boreham, P. Upcroft, J.A. Upcroft, Acta Trop. 56 (1994) 173-194.

[5] S. Moreno, R. Docampo, Environ. Health Perspect. 64 (1985) 199–208.

[6] P.J. Johnson, Parasitol. Today 9 (1993) 183–186.

[7] S. Toumi, M. Hammouda, A. Essid, L. Medimagh, L.B. Slamia, C. Laouani-Kechrid, Med. Maladies Infect. 39 (2009) 906–908.

[8] S. Becker, P. Hoffman, E.R. Houpt, Am. J. Trop. Med. Hyg. 84 (2011) 581–586.

[9] S.M. Siddiqui, A. Salahuddin, A. Azam, Eur. J. Med. Chem. 49 (2012) 411–416.

[10] K. Roy, S. Kar, R.N. Das, A Primer on QSAR/QSPR Modeling, 2015.
[11] H.G. Jeong, Y.W. Lee, Cancer Lett. 134 (1998) 73.
[12] R.D. Cramer, D.E. Patterson, J.D. Bunce, JACS 110 (1988) 5959.
[13] G. Klebe, U. Abraham, T. Mietzner, "Predict Their Biological Activity and Molecular Similarity Indices in a Comparative Analysis (CoMSIA) of Drug Molecules to Correlate" J. Medi. Chem. Vol.37 4130–4146, 1994.
[14] M.H. Shaikh, D.D. Subhedar, L. Nawale, D. Sarkar, F.A. Kalam Khan, J.N. Sangshetti, B.B. Shingate, Med. Chem. Commun. 6 (2015) 1104.
[15] B. Negi, P. Poonan, M. F. Ansari et all, Synthesis, antiamoebic activity and docking studies of metronidazole-triazole-styryl hybrids, *E. J. of Medicinal Chemistry*, S0223-5234(18)30276-9.
[16] M. Clark, R. D. Cramer, and N. Van Opdenbosch, "Validation of the general purpose tripos 5.2 force field's" J. Comput. Chem., vol. 10, no. 8, 982–1012, Dec. 1989.
[17] W. P. Purcell and J. A. Singer, "A brief review and table of semi empirical parameters used in the Hueckel molecular orbital method " J. Chem. Eng. Data, vol. 12, no. 2, 235–246, Apr. 1967.
[18] M. D. M. AbdulHameed, A. Hamza, J. Liu, and C.-G. Zhan, "Combined 3D-QSAR Modeling and Molecular Docking Study on Indolinone Derivatives as Inhibitors of 3-Phosphoinositide- Dependent Protein Kinase-1 " J. Chem. Inf. Model., vol. 48, no. 9, 1760–1772, Sep. 2008.
[19] A. Aouidate, A. Ghaleb, M. Ghamali, et al. J. Struct. Chem. 29 ,1031, 2018.
[20] L. Ståhle, S. Wold, "Experimental design in biomedical research and multivariate data analysis". Prog. Medicinal. Chemistry. Vol.25 , 291–338, 1988.
[21] J. Zheng, G. Xiao, J. Guo, Y. Zheng, H. Gao, S. Zhao, K. Zhang, P. Sun, "Exploring QSARs for 5-Lipoxygenase (5-LO) Inhibitory Activity of 2-Substituted 5-Hydroxyindole-3- Carboxylates by CoMFA and CoMSIA" Chem. Biol. Drug Des, 78, 314–321, 2011.
[22] S. Wold, Quant, Struct. Act. Relat. 10 (1991) 191.
[23] C. Rücker, G. Rücker, M. Meringer, Y-randomization and its variants in QSPR/QSAR, J. Chem. Inf. Model. 47 (2007) 2345–2357.
[24] A. Aouidate, A. Ghaleb, M. Ghamali, A. Ousaa, M. Choukrad, et all "3D- QSAR studies, molecular docking and ADMET evaluation, using thiazolidine derivatives as template to obtain new inhibitors of PIM1 kinase", J. Compu. Biol and Chemist, S1476-9271(18)30036-7.
[25] Dassault Systèmes BIOVIA, Discovery Studio Modeling Environment, Release 2017, San Diego: Dassault Systèmes., (2016). http://accelrys.com/products/collaborative-science/bioviadiscovery-studio/ (accessed February 25, 2017).
[26] W. DeLano, The PyMOL Molecular Graphics System DeLano Scientific, Palo Alto, CA, USA, (2002). http://www.pymol.org (accessed February 25, 2017).
[27] D. Parsonage, F Sheng, K. Hirata, A. Debnath, J. H. McKerrow, S. L. Reed, R. Abagyan, L. B.Poole, L. M. Podust. J. Struct. Biol. 194 (2016) 180-190.
[28] A. Aouidate, A. Ghaleb, M. Ghamali, A. Ousaa, M. Choukrad, A. Sbai, M.Bouachrine, T. Lakhlifi, 3D QSAR studies, molecular docking and ADMET evaluation, using thiazolidine derivatives as template to obtain new inhibitors of PIM1 kinase, *J.Comp. Biol.and Chem.* S1476-9271(18)30036-7.